

# Journal of Materials Chemistry A

Accepted Manuscript



This is an *Accepted Manuscript*, which has been through the Royal Society of Chemistry peer review process and has been accepted for publication.

*Accepted Manuscripts* are published online shortly after acceptance, before technical editing, formatting and proof reading. Using this free service, authors can make their results available to the community, in citable form, before we publish the edited article. We will replace this *Accepted Manuscript* with the edited and formatted *Advance Article* as soon as it is available.

You can find more information about *Accepted Manuscripts* in the [Information for Authors](#).

Please note that technical editing may introduce minor changes to the text and/or graphics, which may alter content. The journal's standard [Terms & Conditions](#) and the [Ethical guidelines](#) still apply. In no event shall the Royal Society of Chemistry be held responsible for any errors or omissions in this *Accepted Manuscript* or any consequences arising from the use of any information it contains.

# A core-shell Pd<sub>1</sub>Ru<sub>1</sub>Ni<sub>2</sub>@Pt/C catalyst with ternary alloy core and Pt monolayer: enhanced activity and stability towards the oxygen reduction reaction by the addition of Ni

Haoxiong Nan, Xinlong Tian, Junming Luo, Dai Dang, Rong Chen, Lina Liu, Xiuhua Li, Jianhuang Zeng, Shijun Liao<sup>1</sup>

The Key Laboratory of Fuel Cell Technology of Guangdong Province & The Key Laboratory of New Energy of Guangdong Universities, School of Chemistry and Chemical Engineering, South China University of Technology, Wushan Road, Guangzhou, Guangdong 510640, China

## Abstract

A core-shell structured catalyst, Pd<sub>1</sub>Ru<sub>1</sub>Ni<sub>2</sub>@Pt/C, with a ternary alloy as its core and a Pt monolayer shell was prepared using a two-stage strategy, in which Pd<sub>1</sub>Ru<sub>1</sub>Ni<sub>2</sub> alloy nanoparticles were prepared by a chemical reduction method, then the Pt monolayer shell was generated via an underpotential deposition method. It was found that the addition of Ni to the core played an important role in enhancing the catalyst's oxygen reduction activity and stability. The optimal molar ratio of Pd:Ru:Ni was about 1:1:2; the catalyst with this optimal ratio had a half-wave potential approximately 65 mV higher than that of PdRu@Pt/C catalyst, and its mass activity was up to 1.06 A mg<sup>-1</sup> Pt, which was more than five times that of a commercial Pt/C catalyst. The catalyst's structure and composition were characterized using X-ray powder diffraction, X-ray photoelectron spectroscopy, transmission electron microscopy, and energy-dispersive X-ray spectrometry. The core-shell structure of the catalyst was demonstrated by the EDS mapping results and supported by the XPS results. We also performed a stability test that confirmed the catalyst's superior stability in comparison to commercial JM Pt/C (20 wt% Pt).

<sup>1</sup> Corresponding author. Tel./Fax: +86 20 8711 3586. E-mail address: [chsjliao@scut.edu.cn](mailto:chsjliao@scut.edu.cn).

**Keywords:** Core–shell structure; alloy nanoparticles; Pt monolayer; electrocatalysts; oxygen reduction reaction

## 1 Introduction

Although proton exchange membrane fuel cells (PEMFCs) are recognized as a promising technology to meet the global energy crisis and address various associated environmental problems, many technical and economic challenges still prevent their large-scale commercialization, one of which is the high cost of platinum.<sup>1</sup> The monolayer core–shell catalyst is, to date, the most promising low-Pt catalyst for pursuing fuel cell commercialization,<sup>2–6</sup> because it can enhance Pt utilization and thereby reduce the amount of Pt required and the cost of PEMFCs. So far, the most commonly used core element for monolayer core–shell catalysts has been palladium,<sup>7–11</sup> but the rising price of Pd is diminishing its appeal.

Recently, alloy nanoparticles combining Pd with other elements have been used as the cores in core–shell catalysts to reduce Pd loading and hence cost. Adzic et al. found that the suitability of PdIr<sup>12</sup> and PdAu<sup>13</sup> as substrates for a Pt monolayer is well documented; nonetheless, per unit, noble metals remain quite expensive.

Previously, we attempted to prepare a core–shell catalyst using the less costly Ru as a core instead of Pd, but the catalyst showed inferior oxygen reduction reaction (ORR) activity to a Pd@Pt/C catalyst if a Pt monolayer was deposited.<sup>14</sup> Again in the interest of reducing cost, in the present study we attempted to prepare a Pt monolayer core–shell catalyst, this time with PdRuNi alloy nanoparticles as the core. After considerable investigation and screening, we found that our optimal catalyst exhibited more than five times higher activity and much better stability than commercial Pt/C. When we examined the effect of the core composition on the catalyst's performance, we found that Ni seemed to be a determining factor in achieving superior performance.

## 2 Experimental

## 2.1 Preparation of carbon-supported PdRuNi nanoparticles

The carbon-supported ternary alloy nanoparticles were prepared as follows. Palladium chloride, ruthenium chloride, and nickel chloride in an atomic ratio of 1:1:2 were added to deionized water to obtain a solution. Next, sodium citrate was added as a complexing agent using a metal/citrate molar ratio of 1:5, after which carbon black XC72R was added to the solution under vigorous stirring. Once the mixture had been purged with high-purity N<sub>2</sub> for 15 minutes, excess NaBH<sub>4</sub> solution (10 wt%) was slowly added, using ultrasonication and under the protection of N<sub>2</sub>. After reaction via ultrasonication for one hour, the mixture was filtered, washed with deionized water three to five times, then dried overnight in a vacuum oven at 50 °C. For comparison, PdRuNi nanoparticles with different molar ratios of Pd:Ru:Ni were prepared using the same procedures as above. The total metal content in each of the samples was 20 wt%.

## 2.2 Synthesis of core-shell catalyst on glassy carbon electrode by UPD

The Pt monolayer core-shell catalyst PdRuNi@Pt/C was prepared on a glassy carbon electrode using an underpotential deposition (UPD) method. First, 5.0 mg carbon-supported ternary PdRuNi alloy nanoparticles were dispersed in 1 mL Nafion ethanol solution (0.1 wt%) via ultrasonication for 30 minutes to make a uniform suspension. Then, 5 μL of the suspension was pipetted onto a glassy carbon disk electrode (5 mm diameter) and dried in air. Next, a Cu monolayer was deposited on the surface of the PdRuNi nanoparticles in a 50 mM H<sub>2</sub>SO<sub>4</sub> + 50 mM CuSO<sub>4</sub> solution by holding the deposition potential at about 0.38 V for one minute, under the protection of high-purity nitrogen. Finally, the electrode was transferred into a solution of 1 mM K<sub>2</sub>PtCl<sub>4</sub> + 50 mM H<sub>2</sub>SO<sub>4</sub> for 10 minutes in a nitrogen atmosphere, during which the Cu monolayer was galvanically replaced by Pt to form a Pt monolayer. The theoretical Pt content in the catalyst was calculated from the UPD charge of Cu, and the real content was determined by inductively coupled plasma atomic emission spectrometry (ICP-AES).

This prepared electrode bearing the core-shell structured catalyst was used, without further treatment, for the subsequent electrochemical performance measurements.

### 2.3 Measurement of the catalysts' electrochemical performance

The electrochemical performance of the various catalysts was measured by cyclic voltammetry (CV) on an electrochemical workstation (Ivium, Netherlands) using a three-electrode electrochemical cell. An Ag/AgCl/KCl (3M) leak-free reference electrode and a Pt wire were used as the reference and counter electrodes, respectively. ORR and hydrogen underpotential deposition (HUPD) measurements were performed in 0.1 M HClO<sub>4</sub> solution saturated with oxygen and 0.05 M H<sub>2</sub>SO<sub>4</sub> solution saturated with nitrogen at room temperature, respectively.

### 2.4 Catalyst characterization

X-ray powder diffraction (XRD) patterns were obtained with a TD-3500 powder diffractometer (Tongda, China) using filtered Cu-K $\alpha$  radiation operating at 40 kV and 30 mA. Scanning transmission electron microscope (STEM) images were recorded on an FEI Titan G2 60-300 operated at 300 kV. X-ray photoelectron spectroscopy (XPS) was performed on an Axis Ultra DLD X-ray photoelectron spectrometer (Kratos, England) employing a monochromated Al-K $\alpha$  X-ray source ( $h\nu = 1486.6$  eV). ICP-AES (Leema PROFILE, America) was used to analyze the trace metal element contents.

## 3 Results and discussion

Fig. 1 shows the XRD patterns of the alloy nanoparticles and the catalysts with various core composition ratios. The diffraction peak located at 20–25° for all of the XRD patterns belongs to the (002) reflection of the Vulcan XC72R carbon black support. From Fig. 1a we can see that although the XRD patterns vary with the composition of the ternary nanoparticles, for all four samples, the diffraction peaks at about 40.0°, 47.0°, 68.0°, and 82.0° correspond to the (111), (200), (220), and (311) crystal planes of the face-centered cubic crystalline structure. This suggests that Ni and Ru atoms either entered the Pd lattice to form a complete alloy or were in amorphous states,<sup>15, 16</sup> the former possibility being most probable.

Peaks are observable at a  $2\theta$  value of about  $33.7^\circ$  for the  $\text{Ni}(\text{OH})_2$  (100) facet in three of the PdRuNi/C samples.<sup>15</sup> The formation of trace nickel hydroxide was due to the reaction of  $\text{Ni}^{2+}$ ,  $\text{NaBH}_4$ , and  $\text{H}_2\text{O}$ .<sup>17</sup> The lattice parameters of  $\text{Pd}_3\text{Ru}_1\text{Ni}_4/\text{C}$ ,  $\text{Pd}_1\text{Ru}_1\text{Ni}_2/\text{C}$ , and  $\text{Pd}_1\text{Ru}_3\text{Ni}_4/\text{C}$  were 3.899, 3.892, and 3.827 Å, calculated from the (111) diffraction plane by Jade software. Clearly, with the decrease in Pd content and the increase in Ru content, the lattice parameter decreased slightly. Meanwhile, we have calculated the alloying degree for the binary and ternary alloy nanoparticles with the methods/equations reported previously.<sup>18, 19</sup> The calculated atomic fractions of Ru ( $\chi_{\text{Ru}}$ ) in the alloys of  $\text{Pd}_3\text{Ru}_1\text{Ni}_4/\text{C}$ ,  $\text{Pd}_1\text{Ru}_1\text{Ni}_2/\text{C}$ ,  $\text{Pd}_1\text{Ru}_3\text{Ni}_4/\text{C}$  and  $\text{Pd}_1\text{Ru}_1/\text{C}$  were 12.1%, 16.1%, 66.9% and 31.4%, respectively. Additionally, the average sizes of  $\text{Pd}_3\text{Ru}_1\text{Ni}_4/\text{C}$ ,  $\text{Pd}_1\text{Ru}_1\text{Ni}_2/\text{C}$ ,  $\text{Pd}_1\text{Ru}_3\text{Ni}_4/\text{C}$ , and  $\text{Pd}_1\text{Ru}_1/\text{C}$  were 4.1, 3.9, 3.6, and 4.6 nm, respectively, based on Scherrer equation calculations, indicating that the particle size increased significantly as the Pd content rose and the Ru content dropped. It should be noted that the addition of Ni may have reduced the alloy particle size.

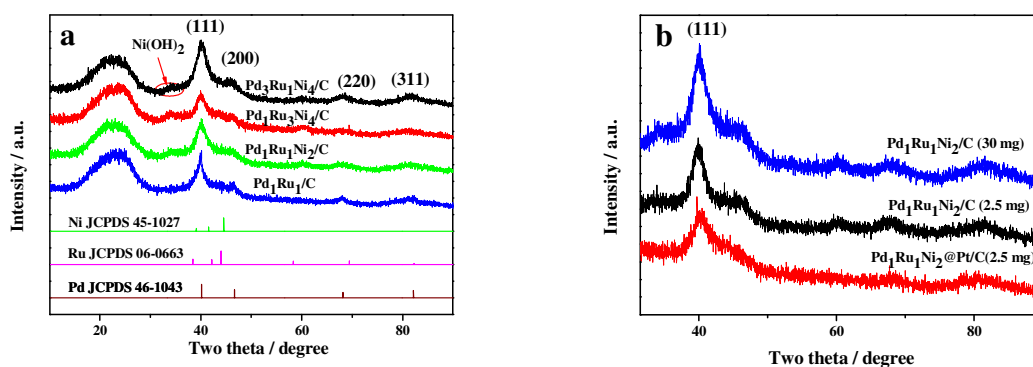
Fig. 1b presents the XRD patterns of  $\text{Pd}_1\text{Ru}_1\text{Ni}_2$  nanoparticles before and after deposition of the Pt shell layer. The (111) diffraction peak of  $\text{Pd}_1\text{Ru}_1\text{Ni}_2@\text{Pt}/\text{C}$  shrank sharply compared to that of  $\text{Pd}_1\text{Ru}_1\text{Ni}_2/\text{C}$ , and the peak at about  $34^\circ$  entirely disappeared; we suggest these effects may have been caused by the dissolution of Ni and  $\text{Ni}(\text{OH})_2$  from the alloy nanoparticles, and the replacement of Ni with Pt during the UPD process.<sup>20</sup> It should be pointed out that no diffraction peaks corresponding to Pt could be observed in the XRD pattern of the  $\text{Pd}_1\text{Ru}_1\text{Ni}_2@\text{Pt}/\text{C}$  catalyst on which the Pt shell layer had been deposited, indicating the formation of an ultra-thin shell—i.e., a monolayer. Such a layer could not generate diffractions.<sup>21, 22</sup>

Table 1 presents the compositions of the samples measured by ICP-AES analysis. The data clearly indicate the deposition of Pt and the dissolution of nickel. After the UPD deposition, the Ni content decreased from ca. 6.8 wt% to 0.30–0.60 wt%. This implies that the Ni alloyed in the PdRuNi nanoparticles could not tolerate the strong acidic solution used for the UPD process. Another reason for the decrease in

Ni content could have been the replacement of Ni with Pt. This possibility is supported by the fact that the Pt content of the catalysts with Ni in the core was higher than that of the catalysts without Ni.

**Table 1** The compositions of  $\text{Pd}_x\text{Ru}_y\text{Ni}_{x+y}/\text{C}$  and  $\text{Pd}_x\text{Ru}_y\text{Ni}_{x+y}@\text{Pt}/\text{C}$  samples measured by ICP-AES

Sample	Pd content / wt%	Ru content / wt%	Ni content / wt%	Pt content / wt%
$\text{Pd}_1\text{Ru}_1\text{Ni}_2/\text{C}$	6.36	5.92	6.92	--
$\text{Pd}_3\text{Ru}_1\text{Ni}_4/\text{C}$	9.36	2.72	6.76	--
$\text{Pd}_1\text{Ru}_3\text{Ni}_4/\text{C}$	3.20	8.92	6.84	--
$\text{RuNi}/\text{C}$	--	12.12	6.88	--
$\text{Pd}_1\text{Ru}_1/\text{C}$	9.52	9.96	--	--
$\text{Pd}_1\text{Ru}_1\text{Ni}_2@\text{Pt}/\text{C}$	6.41	6.00	0.62	4.22
$\text{Pd}_3\text{Ru}_1\text{Ni}_4@\text{Pt}/\text{C}$	9.55	2.87	0.50	4.03
$\text{Pd}_1\text{Ru}_3\text{Ni}_4@\text{Pt}/\text{C}$	3.20	9.11	0.58	3.95
$\text{RuNi}@\text{Pt}/\text{C}$	--	12.39	0.33	4.43
$\text{Pd}_1\text{Ru}_1@\text{Pt}/\text{C}$	8.97	9.60	--	3.09



**Fig. 1** (a) XRD patterns of  $\text{PdRuNi}/\text{C}$  samples with different atomic ratios; (b) XRD patterns of  $\text{Pd}_1\text{Ru}_1\text{Ni}_2/\text{C}$  (2.5 mg, 30 mg) and  $\text{Pd}_1\text{Ru}_1\text{Ni}_2@\text{Pt}/\text{C}$  (2.5 mg).

Fig. 2 presents TEM images of  $\text{Pd}_1\text{Ru}_1\text{Ni}_2/\text{C}$  and  $\text{Pd}_1\text{Ru}_1\text{Ni}_2@\text{Pt}/\text{C}$ . All of the nanoparticles were well dispersed on the carbon support, without apparent aggregation either before or after Pt deposition. As shown in Fig. 2e and Fig. 2g, the  $\text{Pd}_1\text{Ru}_1\text{Ni}_2/\text{C}$  and  $\text{Pd}_1\text{Ru}_1/\text{C}$  nanoparticles exhibited rather narrow size distributions, in the range of 1.35–3.5 and 2.43–4.66 nm, with average diameters of about 2.24 and 3.42 nm, respectively, which are in agreement with the particle results predicted by XRD.

After Pt deposition, the Pd<sub>1</sub>Ru<sub>1</sub>Ni<sub>2</sub>@Pt/C and Pd<sub>1</sub>Ru<sub>1</sub>@Pt/C showed average diameters of ~2.87 and 4.10 nm, respectively (see the size distributions provided in Fig. 2f and Fig. 2h). The diameters of the Pd<sub>1</sub>Ru<sub>1</sub>Ni<sub>2</sub>@Pt/C and Pd<sub>1</sub>Ru<sub>1</sub>@Pt/C nanoparticles increased by ca. 0.63 and 0.68 nm, respectively, indicating that the thickness of the Pt shell layer was ca. 0.3 nm, corresponding to a monolayer of Pt atoms and confirming the formation of core-shell structured catalysts. Fig. 2i shows a high-angle annular dark-field (HAADF) STEM image of a nanoparticle of Pd<sub>1</sub>Ru<sub>1</sub>Ni<sub>2</sub>@Pt/C and the EDS mapping images of its component elements. The EDS mapping images clearly reveal the core-shell structure of the nanoparticles. Strong Pd and Ru signals are present in the central area of the particle, while the Pt (green) signal is mainly evident in the outer area, indicating the particle's core-shell structure. Notably, there was an Ni signal in the particle's inner area, implying that a small amount of nickel—undetectable by XPS—may have remained in the core.

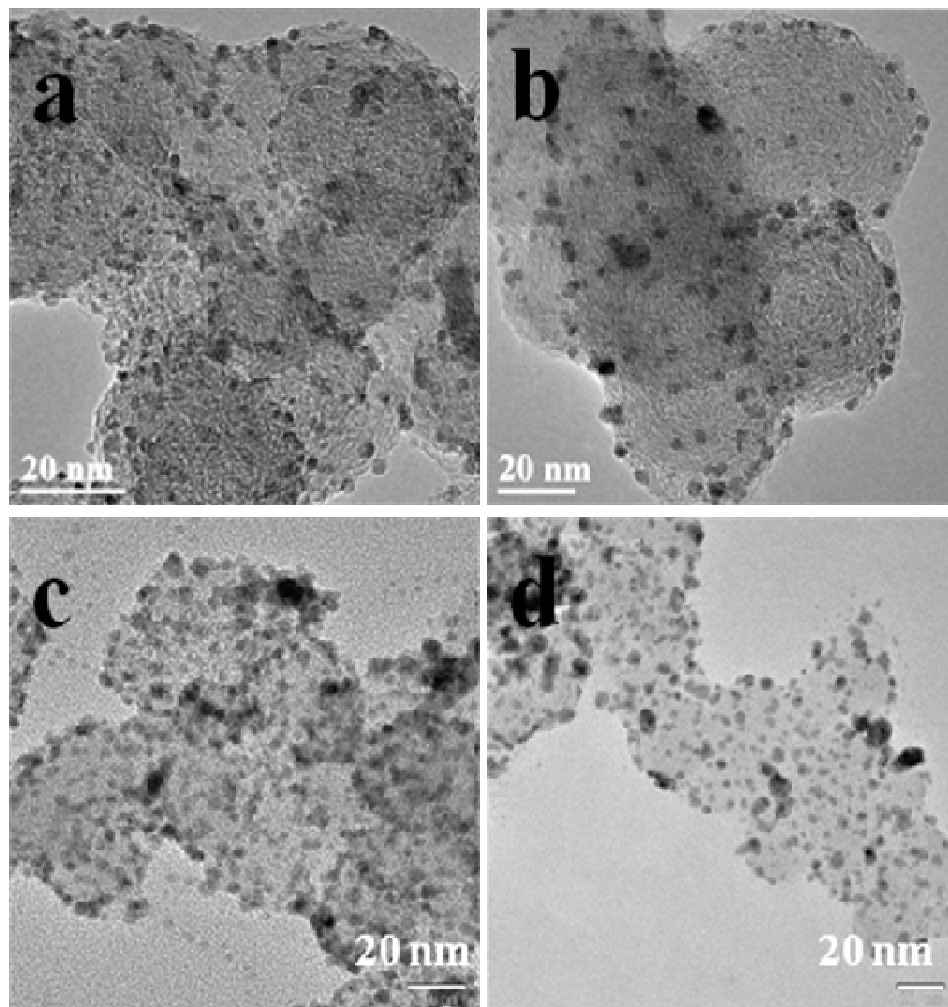
Fig. 3 presents the XPS spectra of Pd<sub>1</sub>Ru<sub>1</sub>Ni<sub>2</sub>/C, Pd<sub>1</sub>Ru<sub>1</sub>Ni<sub>2</sub>@Pt/C, and Pt/C. Fig. 3(a-b) show the XPS survey spectra of Pd<sub>1</sub>Ru<sub>1</sub>Ni<sub>2</sub>/C and Pd<sub>1</sub>Ru<sub>1</sub>Ni<sub>2</sub>@Pt/C. Their surface composition data are listed in Table 2. After Pt deposition, the surface composition clearly changed: no Ni was detectable by XPS, and the surface contents of Pd and Ru decreased sharply compared to Pd<sub>1</sub>Ru<sub>1</sub>Ni<sub>2</sub>/C, even though the Pd/Ru ratio was almost unchanged. This result clearly confirmed that (i) Pt had been deposited on the surface of the Pd<sub>1</sub>Ru<sub>1</sub>Ni<sub>2</sub> nanoparticles and (ii) the nanoparticles' surface had not been completely covered by the Pt monolayer.

We suggest that Ni was not detected in the Pd<sub>1</sub>Ru<sub>1</sub>Ni<sub>2</sub>@Pt/C for two possible reasons: (i) most of the Ni atoms may have been leached out from the Pd<sub>1</sub>Ru<sub>1</sub>Ni<sub>2</sub>/C (or replaced by Pt) in the acidic solution during the UPD process; (ii) the Ni peak may have been covered by the strong Auger peak of F (833.0 eV). According to the ICP-AES results, the first reason was more probable, making the Ni content undetectable by XPS.

The best fits of the Pd (0) 3d spectra (Fig. 3c and Fig. 3d) were obtained using two doublets (Pd 3d<sub>5/2</sub> and 3d<sub>3/2</sub>) with a fixed doublet separation (DS = 5.2 eV). This method revealed that the binding energy of Pd (0) 3d in Pd<sub>1</sub>Ru<sub>1</sub>Ni<sub>2</sub>@Pt/C (336.15 and 341.4 eV) experienced a positive shift of 0.4 eV compared with in

$\text{Pd}_1\text{Ru}_1\text{Ni}_2/\text{C}$  (335.8 and 341.04 eV),<sup>23,24</sup> and the binding energy of Ru 3p in  $\text{Pd}_1\text{Ru}_1\text{Ni}_2@\text{Pt}/\text{C}$  (462.74 and 484.78 eV) underwent a negative shift of 0.3 eV compared with in  $\text{Pd}_1\text{Ru}_1\text{Ni}_2/\text{C}$  (463.02 and 485.23 eV).<sup>25</sup>

The binding energy shifts of Pd and Ru after the deposition of the Pt monolayer may reflect interactions between the Pt shell and the Pd and Ru in the core.



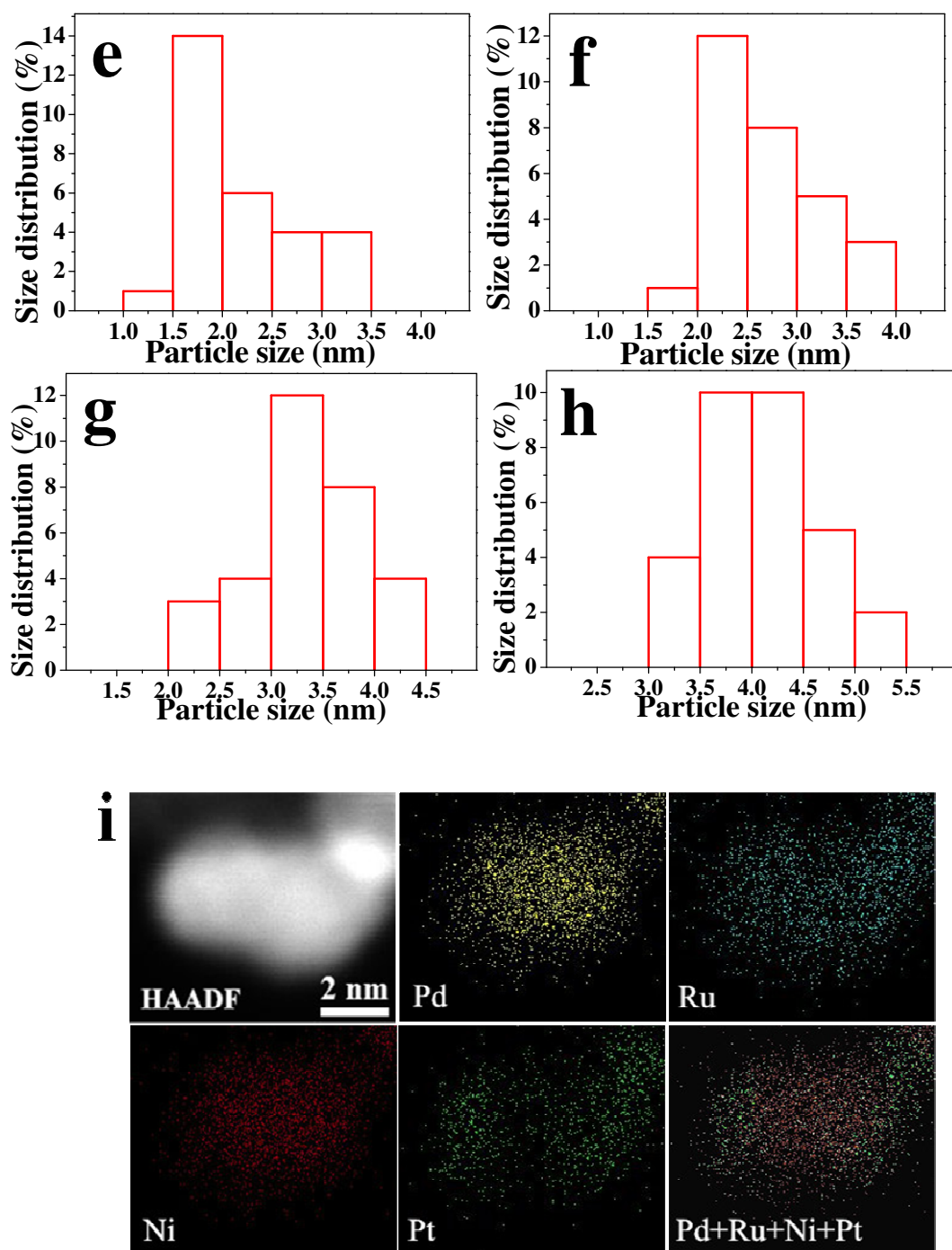


**Fig. 2** TEM images of Pd<sub>1</sub>Ru<sub>1</sub>Ni<sub>2</sub>/C (a), Pd<sub>1</sub>Ru<sub>1</sub>Ni<sub>2</sub>@Pt/C (b), Pd<sub>1</sub>Ru<sub>1</sub>/C (c), and Pd<sub>1</sub>Ru<sub>1</sub>@Pt/C (d); the corresponding particle size histograms of Pd<sub>1</sub>Ru<sub>1</sub>Ni<sub>2</sub>/C (e), Pd<sub>1</sub>Ru<sub>1</sub>Ni<sub>2</sub>@Pt/C (f), Pd<sub>1</sub>Ru<sub>1</sub>/C (g), and Pd<sub>1</sub>Ru<sub>1</sub>@Pt/C (h); HAADF STEM image of Pd<sub>1</sub>Ru<sub>1</sub>Ni<sub>2</sub>@Pt/C, EDS mapping with signals attributed to Pd, Ru, Ni, and Pt, respectively, and overlap of Pd, Ru, Ni, and Pt EDS signals (i).

In addition, the binding energies of Pt 4f for Pd<sub>1</sub>Ru<sub>1</sub>Ni<sub>2</sub>@Pt/C and Pd<sub>1</sub>Ru<sub>1</sub>@Pt/C shifted negatively by 0.4 and 0.2 eV, respectively, compared with the JM Pt/C catalyst. This demonstrates that Pd<sub>1</sub>Ru<sub>1</sub>Ni<sub>2</sub>@Pt/C

had stronger electron interactions between the alloy core and the Pt shell than Pd<sub>1</sub>Ru<sub>1</sub>@Pt/C, due to the addition of Ni. The negative shift in the Pt 4f binding energy suggests that the Pt nanoparticles obtained electrons from the alloy core, resulting in weakened interactions between the Pt atoms and intermediate oxide species. Thus, the ORR performance was enhanced.<sup>26</sup>

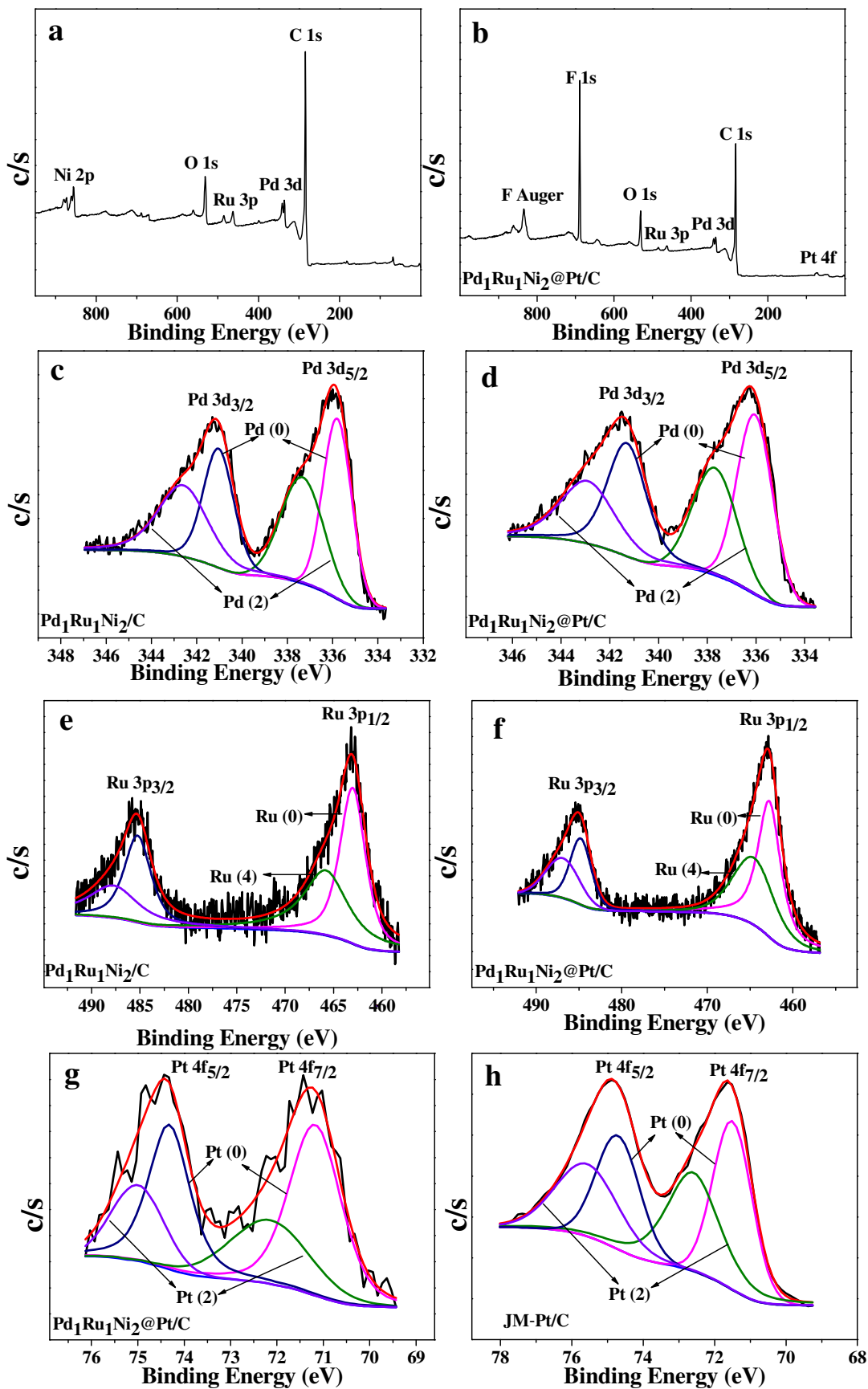
**Table 2** The surface compositions of the Pd<sub>1</sub>Ru<sub>1</sub>Ni<sub>2</sub>/C and Pd<sub>1</sub>Ru<sub>1</sub>Ni<sub>2</sub>@Pt/C samples, measured by XPS.

Sample	Concentration (at%)						
	Pd 3d	Ru 3p	Ni 2p	Pt 4f	C 1s	O 1s	F 1s*
Pd <sub>1</sub> Ru <sub>1</sub> Ni <sub>2</sub> /C	1.68	1.56	2.66	–	83.25	0.8	–
Pd <sub>1</sub> Ru <sub>1</sub> Ni <sub>2</sub> @Pt/C	0.78	0.66	–	0.48	56.86	1.8	29.42

\*This may have been introduced from the Nafion used as a binder in the UPD process.

**Table 3** The theoretical and actual deposited contents of Pt for Pd<sub>x</sub>Ru<sub>y</sub>Ni<sub>x+y</sub>@Pt/C catalysts

Sample	Theoretical content of Pt / wt%	Actual content of Pt / wt%
Pd <sub>1</sub> Ru <sub>1</sub> Ni <sub>2</sub> @Pt/C	3.26	4.22
Pd <sub>3</sub> Ru <sub>1</sub> Ni <sub>4</sub> @Pt/C	3.10	4.03
Pd <sub>1</sub> Ru <sub>3</sub> Ni <sub>4</sub> @Pt/C	2.70	3.95
RuNi@Pt/C	3.63	4.43
Pd <sub>1</sub> Ru <sub>1</sub> @Pt/C	2.54	3.09



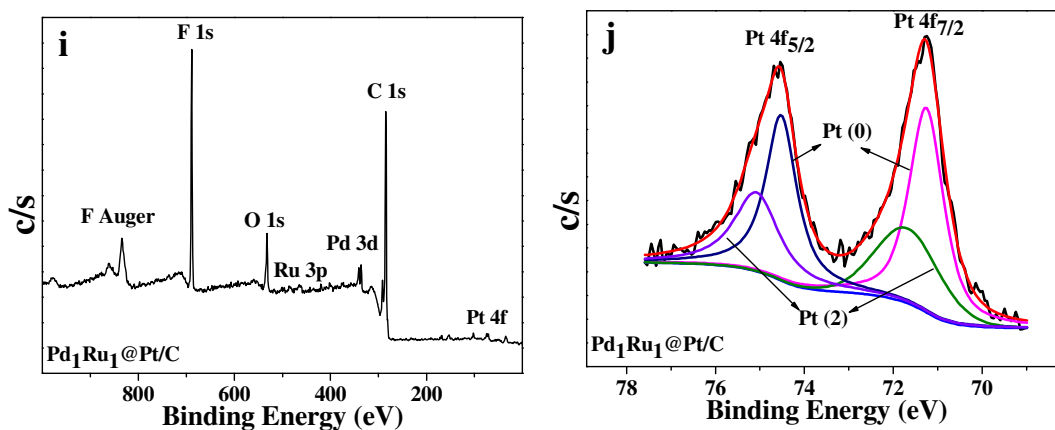


**Fig. 3** (a) XPS survey spectra and corresponding high-resolution spectra of (c) Pd 3d and (e) Ru 3p for Pd<sub>1</sub>Ru<sub>1</sub>Ni<sub>2</sub>/C; (b) survey spectra and corresponding high-resolution spectra of (d) Pd 3d, (f) Ru 3p, and (g) Pt 4f for Pd<sub>1</sub>Ru<sub>1</sub>Ni<sub>2</sub>@Pt/C; (h) Pt 4f in JM Pt/C; (i) survey spectrum and corresponding high-resolution spectrum of (j) Pt 4f for Pd<sub>1</sub>Ru<sub>1</sub>@Pt/C.

Fig. 4 shows the CV curves for alloy nanoparticles of various compositions before and after Pt deposition, in deaerated 0.05 M H<sub>2</sub>SO<sub>4</sub> at a scan rate of 50 mV s<sup>-1</sup>. Pd<sub>1</sub>Ru<sub>1</sub>Ni<sub>2</sub>/C and Pd<sub>1</sub>Ru<sub>1</sub>/C clearly exhibited almost the same CV curves, apart from the slight positive shift in the position of the metal oxide reduction peak in Pd<sub>1</sub>Ru<sub>1</sub>Ni<sub>2</sub>/C; both had almost the same hydrogen reduction and oxidation peaks.

As is evident in Fig. 4c, Pd<sub>1</sub>Ru<sub>1</sub>Ni<sub>2</sub>@Pt/C exhibited obviously larger hydrogen reduction and oxidation peaks than Pd<sub>1</sub>Ru<sub>1</sub>@Pt/C, which may have been for one of two reasons: (i) the Pt content of the Ni-containing sample may have been slightly higher than that of the sample without Ni if some of the Ni had been replaced with Pt; (ii) there may have been a stronger interaction between the Pt shell and the Pd and Ru in the Ni-containing sample due to the existence of low-coordinating Pd and Ru atoms caused by the dissolution of Ni.

To test these possibilities, we analyzed the two samples' Pt content and found that in Pd<sub>1</sub>Ru<sub>1</sub>Ni<sub>2</sub>@Pt/C, it was 4.22 wt%, 26.8% higher than in Pd<sub>1</sub>Ru<sub>1</sub>@Pt/C. As Fig. 4d shows, the deposition reduction peak and

oxidation peak related to the Cu UPD were clearly observable for Pd<sub>1</sub>Ru<sub>1</sub>/C and Pd<sub>1</sub>Ru<sub>1</sub>Ni<sub>2</sub>/C. The peak area of Pd<sub>1</sub>Ru<sub>1</sub>Ni<sub>2</sub>/C was higher than that of Pd<sub>1</sub>Ru<sub>1</sub>/C.

We also calculated the theoretical Pt content in all of our Pt deposited samples, then measured their real Pt content using ICP-AES. As shown in Table 3, the actual Pt loadings (i.e., the actual deposited Pt amounts) were 17–32% higher than the theoretical calculated amounts, for all of the samples. However, the amounts of Pt in Ni-containing samples are obviously larger than in samples without Ni, verifying the idea that in those instances, Ni was replaced by Pt.

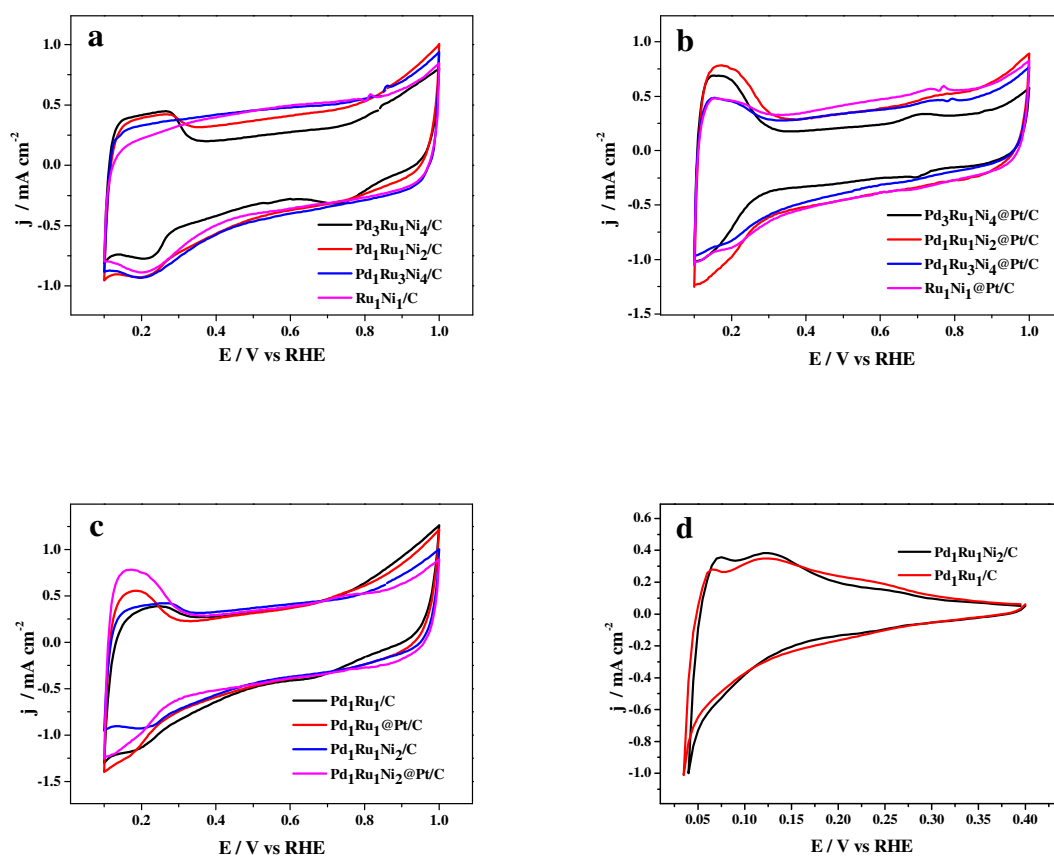


**Fig. 4** (a), (b), and (c): CV curves for the samples before and after UPD, recorded in deaerated 0.05 M H<sub>2</sub>SO<sub>4</sub> at a scan rate of 50 mV s<sup>-1</sup>; (d) CV curves for Pd<sub>1</sub>Ru<sub>1</sub>/C and Pd<sub>1</sub>Ru<sub>1</sub>Ni<sub>2</sub>/C in deaerated 0.05 M H<sub>2</sub>SO<sub>4</sub> + 0.05 M CuSO<sub>4</sub> solution at a scan rate of 10 mV s<sup>-1</sup>.

Fig. 5 presents the ORR polarization curves before and after Pt deposition on all of the samples and on JM Pt/C, in oxygen-saturated 0.1 M HClO<sub>4</sub> solution. As is evident in Fig. 5a, all of the alloy samples

showed ORR activity before Pt deposition, with Pd<sub>3</sub>Ru<sub>1</sub>Ni<sub>4</sub>/C exhibiting the best ORR activity and RuNi/C the worst.

After the UPD of Pt, all of the catalysts showed greatly enhanced ORR performance, Pd<sub>1</sub>Ru<sub>1</sub>Ni<sub>2</sub>@Pt/C exhibiting the best with a half-wave potential about 153 mV higher than that of Pd<sub>1</sub>Ru<sub>1</sub>Ni<sub>2</sub>/C (Fig. 5c). Clearly, Pt deposition significantly enhanced the catalyst's ORR performance.

Further, the catalysts with cores containing Ni exhibited superior ORR performance to those containing no Ni. Pd<sub>1</sub>Ru<sub>1</sub>Ni<sub>2</sub>@Pt/C achieved the best ORR activity, even superior to that of commercial JM Pt/C, with the onset potential and half-wave potential reaching 0.90–1.05 V and 0.89 V, respectively. However, having too much Ru in the core may have resulted in inferior ORR activity, as indicated in Fig. 5b, where Pd<sub>1</sub>Ru<sub>3</sub>Ni<sub>4</sub>@Pt/C shows the worst performance. This again confirms that Ru may not be a good candidate for the core in Pt monolayer core–shell catalysts.

The Pt mass activity of Pd<sub>1</sub>Ru<sub>1</sub>Ni<sub>2</sub>@Pt/C and Pd<sub>3</sub>Ru<sub>1</sub>Ni<sub>4</sub>@Pt/C reached 1.06 and 0.93 A mg<sup>-1</sup> Pt, respectively, at 0.9 V/RHE, whereas their specific activity was 0.57 and 0.45 mA cm<sup>-2</sup>, respectively. The mass activity of Pd<sub>1</sub>Ru<sub>1</sub>Ni<sub>2</sub>@Pt/C was 5.2 times that of Pd<sub>1</sub>Ru<sub>1</sub>@Pt/C and over five times that of JM Pt/C. Based on these results, we can conclude that (i) the high mass activity of Pd<sub>1</sub>Ru<sub>1</sub>Ni<sub>2</sub>@Pt/C may be strong evidence for the formation of a core–shell structured catalyst and (ii) the addition of Ni may have played an important role in performance enhancement.

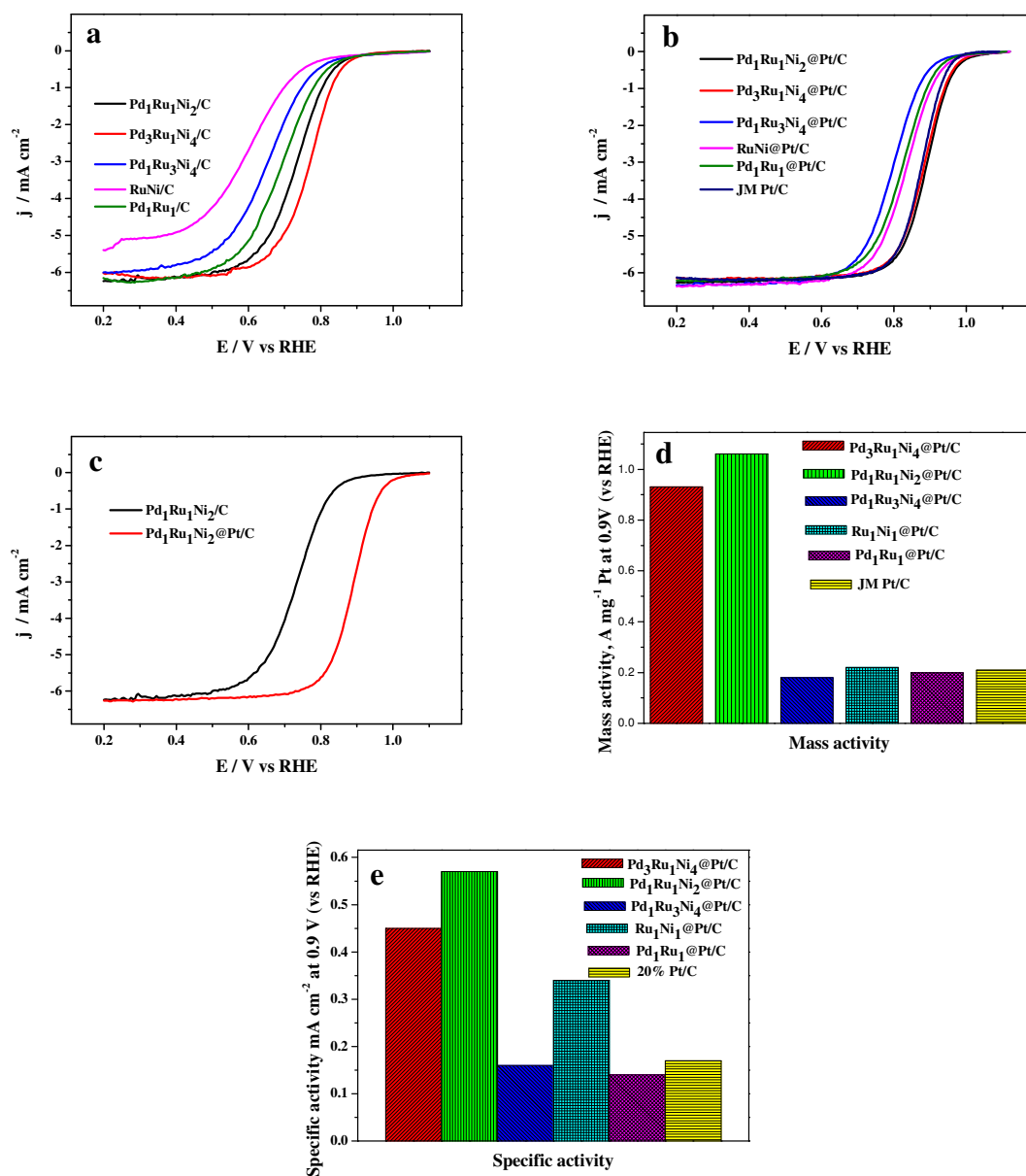


**Fig. 5** (a), (b), (c): Polarization curves for the ORR at 1600 rpm before and after Pt deposition on all of the samples in oxygen-saturated 0.1 M HClO<sub>4</sub>, at a scan rate of 10 mV s<sup>-1</sup>; (d), (e) mass activity and specific activity for these electrocatalysts.

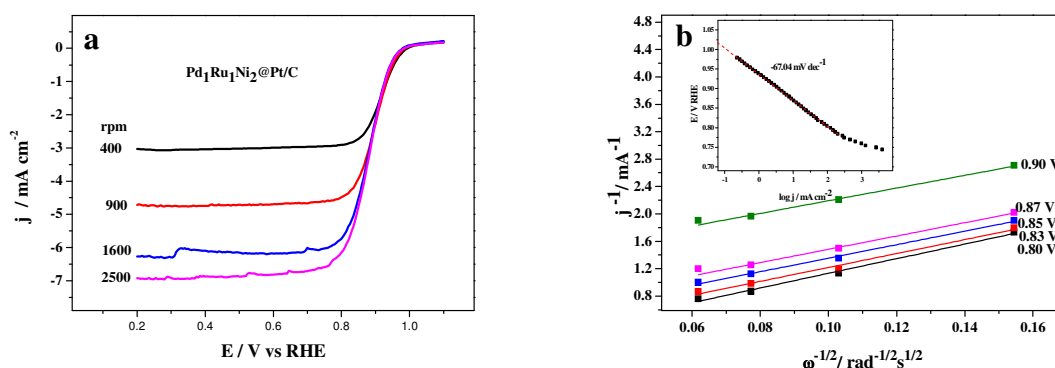


**Fig. 6** (a) Polarization curves of Pd<sub>1</sub>Ru<sub>1</sub>Ni<sub>2</sub>@Pt/C, obtained with a rotating disk electrode for the ORR in 0.1 M HClO<sub>4</sub> solution; (b) Koutecky–Levich plots at different potentials using the data obtained from Pd<sub>1</sub>Ru<sub>1</sub>Ni<sub>2</sub>@Pt/C (inset: Tafel plot from the kinetic current).

Fig. 6a presents the ORR polarization plots of Pd<sub>1</sub>Ru<sub>1</sub>Ni<sub>2</sub>@Pt/C calculated in oxygen-saturated 0.1 M HClO<sub>4</sub> at different rotation speeds (400–2500 rpm), while the Koutecky–Levich plots obtained from Fig. 6a are shown in Fig. 6b. We used the average slopes of the Koutecky–Levich plots and the equation  $B = 0.62nFAD_{O_2}^{2/3} \nu^{-1/6} C_{O_2}$  (where  $D_{O_2} = 1.93 \times 10^{-5} \text{ cm}^2 \text{ s}^{-1}$ ,  $\nu = 1.009 \times 10^{-2} \text{ cm}^2 \text{ s}^{-1}$ ,  $C_{O_2} = 1.26 \times 10^{-3} \text{ mol L}^{-1}$ ,  $F$  is the Faraday constant, and  $A$  is the geometric area of the electrode).<sup>27</sup> The electron transfer number,  $n = 4.3$ , was derived from the slopes of the Koutecky–Levich plots at various potentials and confirms that the ORR on Pd<sub>1</sub>Ru<sub>1</sub>Ni<sub>2</sub>@Pt/C predominantly followed the four-electron exchange pathway. What is more, the linearity and parallelism of the plots shown in Fig. 6b are signs of first-order kinetics with respect to molecular oxygen.<sup>28</sup> The Tafel plot obtained from the kinetic current,  $j_k$ , is shown in the inset of Fig. 6b. The plot is linear, with a slope of approximately  $-67.04 \text{ mV dec}^{-1}$  above 0.80 V.

### 3.3 Stability

The Pd<sub>1</sub>Ru<sub>1</sub>Ni<sub>2</sub>@Pt/C core–shell structured catalyst exhibited excellent stability, as shown in Fig. 7a. After 10,000 CV cycles in nitrogen-saturated 0.05 mol L<sup>-1</sup> H<sub>2</sub>SO<sub>4</sub> solution, the decay in the electrochemical active surface area (ECSA) was 18.5%, compared to 79.8% and 28.1% for Pd<sub>1</sub>Ru<sub>1</sub>@Pt/C and JM Pt/C, respectively. Furthermore, after 10,000 ORR scans, the ORR performance decay of Pd<sub>1</sub>Ru<sub>1</sub>Ni<sub>2</sub>@Pt/C was 27.8%, whilst for JM Pt/C and Pd<sub>1</sub>Ru<sub>1</sub>@Pt/C it was 28.1% and 70%, respectively, indicating the better stability of our core–shell structured catalyst with a Pt monolayer and a ternary alloy core.

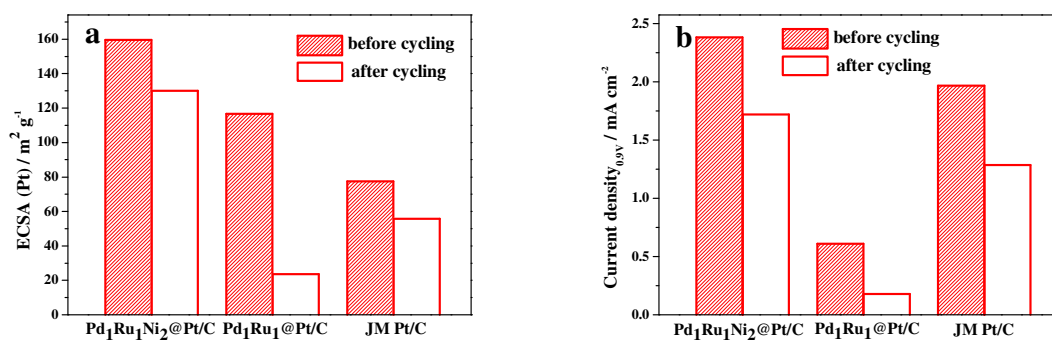


**Fig. 7** ECSA and current density at 0.9 V vs. RHE of the ORR for Pd<sub>1</sub>Ru<sub>1</sub>Ni<sub>2</sub>@Pt/C, Pd<sub>1</sub>Ru<sub>1</sub>@Pt/C, and JM Pt/C at the initial scan and after 10,000 scans.

Clearly, the core-shell catalyst with a Ni-containing core exhibited far superior ORR activity and stability compared to one containing no Ni. Why did Ni play such an important role in the alloy core? As discussed above, one reason could be the catalyst's higher Pt content, because Pt ions may have replaced Ni during UPD. However, for Pd<sub>1</sub>Ru<sub>1</sub>Ni<sub>2</sub>@Pt/C and Pd<sub>1</sub>Ru<sub>1</sub>@Pt/C, the Pt content difference was only 26.8%, so it is difficult to explain the five-fold higher activity and three-fold higher stability of Pd<sub>1</sub>Ru<sub>1</sub>Ni<sub>2</sub>@Pt/C on that basis alone. Ni dissolution would have generated a porous structure in the alloy nanoparticles, resulting in many Pd atoms with low coordination; once the Pt atoms were deposited on these unsaturated Pd or Ru atoms, strong electronic interaction/transfer would have occurred, and this may be the most important explanation for the high degree of performance enhancement in the Ni-containing catalyst. Indeed, the XPS results support this suggestion, as in Pd<sub>1</sub>Ru<sub>1</sub>Ni<sub>2</sub>@Pt/C, the Pt 4f binding energy shifted more than in Pd<sub>1</sub>Ru<sub>1</sub>@Pt/C.

With respect to stability, the porous structure generated by the dissolution of Ni may have led most of the Pt to be deposited on the interior (rather than the exterior) surface of the alloy nanoparticles, resulting in higher catalyst stability. Another cause could have been stronger interaction between the Pt and the low-coordinated Pd or Ru, which might have resulted in a stronger binding force between the Pt and the Pd and/or Ru.

## 4 Conclusions

A high-performance core-shell structured catalyst with a Pt monolayer shell and a ternary alloy nanoparticle core was successfully prepared via a UPD method. The catalyst exhibited very high ORR activity and good stability. Adding Ni to the core played an important role in significantly enhancing the catalyst's ORR performance. Our catalyst with the optimal Pd:Ru:Ni ratio of 1:1:2, Pd<sub>1</sub>Ru<sub>1</sub>Ni<sub>2</sub>@Pt/C, exhibited an ORR performance 5.2 times higher than that of PdRu@Pt/C. Further, the catalyst demonstrated excellent stability after 10,000 ORR scans, with a performance decay of only 27.8%, compared to 70% for PdRu@Pt/C. EDS mapping results revealed the catalyst's core-shell structure.

## Acknowledgements

This work was supported by the National Science Foundation of China (NSFC Project Nos. 21276098, 21476088, 51302091, U1301245), the Ministry of Science and Technology of China (Project No. 2012AA053402), the Guangdong Natural Science Foundation (Project No. S2012020011061), and the Department of Education of Guangdong Province (Project No. 2013CXZDA003).

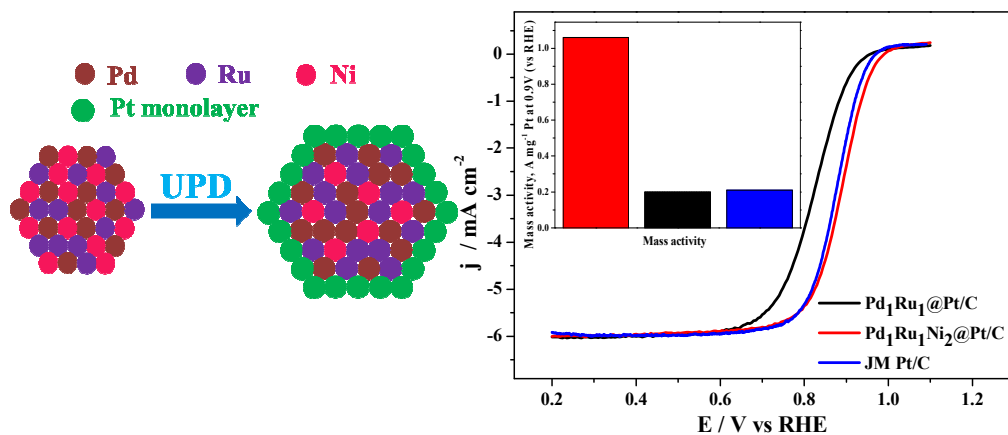
## References

1. A. Morozan, B. Josselme and S. Palacin, *Energy & Environmental Science*, 2011, **4**, 1238-1254.
2. S. Brankovic, J. Wang and R. Adžić, *Surface Science*, 2001, **474**, L173-L179.
3. S. R. Branković, J. Wang and R. R. Adžić, *Journal of the Serbian Chemical Society*, 2001, **66**, 887-898.
4. K. Sasaki, Y. Mo, J. Wang, M. Balasubramanian, F. Uribe, J. McBreen and R. Adzic, *Electrochimica Acta*, 2003, **48**, 3841-3849.
5. E. Skúlason, G. S. Karlberg, J. Rossmeisl, T. Bligaard, J. Greeley, H. Jónsson and J. K. Nørskov, *Physical Chemistry Chemical Physics*, 2007, **9**, 3241-3250.

6. K. A. Kuttiyiel, K. Sasaki, D. Su, M. B. Vukmirovic, N. S. Marinkovic and R. R. Adzic, *Electrochimica Acta*, 2013, **110**, 267-272.
7. R. R. Adzic, J. Zhang, K. Sasaki, M. B. Vukmirovic, M. Shao, J. Wang, A. U. Nilekar, M. Mavrikakis, J. Valerio and F. Uribe, *Topics in Catalysis*, 2007, **46**, 249-262.
8. K. Sasaki, J. Zhang, J. Wang, F. Uribe and R. Adzic, *Research on chemical intermediates*, 2006, **32**, 543-559.
9. R. R. Adzic, *Electrocatalysis*, 2012, **3**, 163-169.
10. K. Gong, J. Park, D. Su and R. R. Adzic, *Journal of Solid State Electrochemistry*, 2014, **18**, 1171-1179.
11. D. Dang, H. Zou, Z. a. Xiong, S. Hou, T. Shu, H. Nan, X. Zeng, J. Zeng and S. Liao, *ACS Catalysis*, 2015, **5**, 4318-4324.
12. S. L. Knupp, M. B. Vukmirovic, P. Haldar, J. A. Herron, M. Mavrikakis and R. R. Adzic, *Electrocatalysis*, 2010, **1**, 213-223.
13. K. Sasaki, H. Naohara, Y. Choi, Y. Cai, W.-F. Chen, P. Liu and R. R. Adzic, *Nature communications*, 2012, **3**, 1115.
14. L. J. Yang, M. B. Vukmirovic, D. Su, K. Sasaki, J. A. Herron, M. Mavrikakis, S. J. Liao and R. R. Adzic, *J Phys Chem C*, 2013, **117**, 1748-1753.
15. S. Shen, T. Zhao, J. Xu and Y. Li, *Energy & Environmental Science*, 2011, **4**, 1428-1433.
16. Z. Liu, X. Zhang and S. W. Tay, *Journal of Solid State Electrochemistry*, 2012, **16**, 545-550.
17. L. Cao, Y. Ni, M. Wang and X. Ma, *Rsc Advances*, 2013, **3**, 3585-3591.
18. E. Antolini, F. Colmati and E. Gonzalez, *Journal of Power Sources*, 2009, **193**, 555-561.
19. F. Colmati, E. Antolini and E. Gonzalez, *J Alloy Compd*, 2008, **456**, 264-270.
20. Y. Zhang, C. Ma, Y. Zhu, R. Si, Y. Cai, J. X. Wang and R. R. Adzic, *Catalysis Today*, 2013, **202**, 50-54.

21. W.-P. Zhou, K. Sasaki, D. Su, Y. Zhu, J. X. Wang and R. R. Adzic, *The Journal of Physical Chemistry C*, 2010, **114**, 8950-8957.
22. H. Nan, X. Tian, L. Yang, T. Shu, H. Song and S. Liao, *Journal of Nanomaterials*, 2015, **2015**.
23. C. Du, M. Chen, W. Wang and G. Yin, *ACS applied materials & interfaces*, 2010, **3**, 105-109.
24. Y.-Y. Feng, Z.-H. Liu, Y. Xu, P. Wang, W.-H. Wang and D.-S. Kong, *Journal of Power Sources*, 2013, **232**, 99-105.
25. J. C. Calderona, G. Garcia, L. Calvillo, J. L. Rodriguez, M. J. Lazaro and E. Pastor, *Appl Catal B-Environ*, 2015, **165**, 676-686.
26. G. Wang, B. Huang, L. Xiao, Z. Ren, H. Chen, D. Wang, H. c. D. Abruña, J. Lu and L. Zhuang, *Journal of the American Chemical Society*, 2014, **136**, 9643-9649.
27. K. Sasaki, L. Zhang and R. Adzic, *Physical Chemistry Chemical Physics*, 2008, **10**, 159-167.
28. N. Anastasijević, V. Vesović and R. Adžić, *Journal of electroanalytical chemistry and interfacial electrochemistry*, 1987, **229**, 305-316.

## Graphical abstract



A platinum monolayer core-shell structured catalyst with a ternary alloy nanoparticle as core is prepared by an underpotential deposition method, the catalyst exhibits excellent oxygen reduction reaction activity, the half-wave is about 65 mV higher than that of PdRu@Pt/C catalyst in 0.1 M HClO<sub>4</sub>. Furthermore, it also presents outstanding stability, after 10,000 ORR scans, the performance decay is only 27.8%, compared the 70 % of PdRu@Pt/C catalyst.